Available online at www.sciencedirect.com
ScienceDirect
Trans. Nonferrous Met. Soc. China 33(2023) 1742−1754
Transactions of Nonferrous Metals Society of China
www.tnmsc.cn

Ageing precipitation sequence and effect of ω and secondary α phases on tensile properties of metastable β Ti−6Cr−5Mo−5V−4Al alloy

Wei ZHOU[1], Chang WANG[1], Ji-xiong LIU[2], Si-yun LI[3], Hui-qun LIU[1,3]

1. School of Materials Science and Engineering, Central South University, Changsha 410083, China;
2. Baoti Group Ltd., Baoji 721014, China;
3. State Key Laboratory of Powder Metallurgy, Central South University, Changsha 410083, China

Received 20 January 2022; accepted 6 April 2022

Abstract: The ageing precipitation sequence and the relationship between microstructure and tensile properties of metastable β titanium alloy Ti−6Cr−5Mo−5V−4Al during solution and ageing were investigated. Ageing from 400 to 450 °C, isothermal ω phase (ω_{iso}) precipitated in the alloy, resulting in high hardening and brittle fracture. After ageing at 450−500 °C, ω_{iso} phase was gradually replaced by secondary α phase (α_s) with the ageing time increasing. At higher ageing temperature (580−600 °C), ω_{iso} precipitation was suppressed, and α_s phase precipitated directly from β phase. The yield strength of sample aged at 450 °C for 12 h was 1368 MPa and the elongation was 5.5% due to ω_{iso} precipitation. The yield strength of sample aged at 600 °C for 12 h was 1108 MPa and the elongation was improved to 15.4% due to the precipitation and coarsening of α_s phase.

Key words: metastable β-Ti alloy; precipitation sequence; ω phase; α_s phase; strength; ductility

1 Introduction

Titanium alloys are particularly competitive in the aerospace industry due to their low density, high specific strength, good corrosion resistance, and low thermal conductivity [1−3]. Compared with other titanium alloys, metastable β titanium alloys are superior in aeronautic applications, such as landing gear and wing structures, owing to their high yield strength, good fatigue, and crack propagation properties [4−6].

The precipitation and growth of phase in β titanium alloy have a significant effect on the balance of strength and toughness [7]. When the solution temperature is lower than the β transus temperature, the formation of primary α phase (α_p) increases the strength and ductility. The secondary α phase (α_s), which is responsible for the high strength of β Ti alloys, precipitates from matrix ageing. The strength of β titanium alloy is closely related to the size, volume, morphology and distribution of α phase [8−10]. Various transient phases, including α', α'', ω and β' phases could precipitate from β phase and influence the precipitation of α phase, depending on the chemical elements and phase-transition driving forces [11−14]. The athermal ω phase (ω_{ath}) forms by non-diffusion process, such as water quenching, whereas isothermal ω phase (ω_{iso}) forms during ageing [15]. Notably, the ω_{iso} has been widely investigated and generally results in unexpected embrittlement [16−18]. WAN et al [19] found that the quenched Ti−19Nb−1.5Mo−4Zr−8Sn alloy containing small amount of α' phase possesses low elastic modulus and sufficient fracture plasticity, but low tensile strength. However, during low-temperature ageing, the elastic modulus and strength of the alloy increase sharply, but the plasticity decreases. This is attributed to the precipitation of ω phase. With the

Corresponding author: Hui-qun LIU, Tel: +86-731-88836320, E-mail: liuhuiqun@csu.edu.cn
DOI: 10.1016/S1003-6326(23)66218-1

increasing ageing temperature and time, the ω phase gradually transformed into α phase, which promotes the increase of plasticity and decrease of tensile strength. YI et al [20] found that ω_{ath} precipitates from supersaturated solid solution β phase in Ti−7Nb−10Mo alloy after solution treatment. In the temperature range of 350−400 °C, the nano ω_{ath} phase gradually changes to ω_{iso} phase during ageing. The dissolution of ω_{iso} and precipitation of α phase are enhanced at higher ageing temperatures.

One of the most effective methods known to control the microstructure of metastable β titanium alloys is solution and ageing treatment [21−23]. The solution treatment (ST) could partially or completely dissolve α phase into matrix, thus, the oversaturated β titanium alloy exhibits good elongation, but low strength [24]. In addition, the strength of metastable β titanium alloy could be significantly improved by the precipitation of secondary phase during ageing [25−27]. Decreasing the size of α_s phase or increasing its volume fraction significantly increases the strength of metastable β titanium alloy [23]. Therefore, an insightful analysis of the effect of microstructure on mechanical properties of alloys during heat treatment is extremely useful for material engineers and designers to optimize heat-treatment strategies and control the microstructure [28,29]. WU and ZHAN [23] investigated the volume fraction of α_p, which decreased with the increase of solution temperature and time, and disappeared when the temperature rose above β transus temperature. ZHU et al [26] studied the multi-scale lamellar structure of Ti−5Al−4Zr−8Mo−7V alloy prepared by BASCA (β annealing + slow cooling + ageing) treatment, and the combination of strength and toughness was improved. DU et al [9] studied the precipitation of α_s phase in Ti−10Mo−6Zr−4Sn−3Nb alloy, and found that only small volume fraction of α_s phase precipitated around β grain boundary during low-temperature ageing, and the volume fraction in the β matrix increased sharply with ageing time.

In this study, the age hardening behavior of Ti−6Cr−5Mo−5V−4Al alloy was investigated systematically [27,30], in order to determine the microstructural evolution and precipitation sequence during ST and ageing, as well as their effects on the strength and ductility of the alloy. This work could contribute to the method for optimizing the microstructure for improving the combination of strength and ductility to satisfy aerospace application [31].

2 Experimental

Ti−6Cr−5Mo−5V−4Al alloy used in this study was a hot-forged bar provided by Baoti Group. The metallographic method was used to identify the β transus temperature of the alloy as 810 °C. The STA (solution and ageing treatment) heat-treatment process is shown in Fig. 1(a). The solution was treated at 800 °C (below the β transus temperature) for 2 h and air cooled. The ageing temperature was set to 300, 350, 400, 450, 500, 550, 580, or 600 °C with ageing time from 5 min to 120 h, followed by air cooling. The hardness of the alloy was measured using an HV−10B micro Vickers hardness tester. During measurement, a load of 1 kg was applied for continuous pressure period of 15 s. Seven points were measured and averaged for each sample to obtain the average hardness value.

Phase components of alloy at different status were carried out by X-ray diffraction (XRD) using a Rigaku D/Max 2500 X-ray diffractometer with Cu as radiation source and a graphite monochromator. The XRD measurement was taken at operating voltage of 40 kV, current of 250 mA, with a rotating target. The scanning rate was 4 (°)/min, and the diffraction angle range was 2θ=30°−80°. The microstructure of the alloy was observed by scanning electron microscopy (SEM) and transmission electron microscopy (TEM). SEM observations were performed using Quanta-200 environmental scanning electron microscope. The volume fraction and size of α precipitates were statistically analyzed by using Image-J software. The average number of the precipitates was measured over 100 phases for each sample to obtain the average statistical value. TEM observations were performed using Tecnai G2 F20 and Titan 80−300 transmission electron microscopes with operating voltages of 200 and 300 kV, respectively. The composition of the double spray electrolyte was perchloric acid: *n*-butanol: methanol = 5:35:60 (mass ratio). The tensile specimen dimensions used for evaluating the mechanical properties were determined in accordance with standard GB/T228—2010, as shown in Fig. 1(b). Uniaxial tensile

tests were conducted by MTS Landmark with a strain rate of 2.5×10^{-3} s^{-1} at room temperature (25 °C). The arithmetic mean value of the test results of three samples was taken as the final result in each experiment.

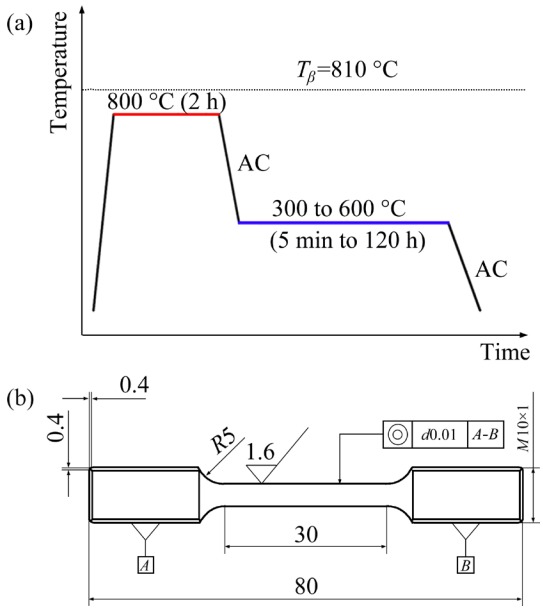

Fig. 1 Schematic illustration of heat treatment process (a), and schematic of tensile specimen (b) (unit: mm)

3 Results and discussion

3.1 Microstructure of ST alloy

Figure 2 shows the microstructure and corresponding XRD pattern of the alloy after ST at 800 °C for 2 h followed by air cooling. As shown in Fig. 2(a), the alloy solution treated at α/β phase region consists of β phase and spherical primary α phase (α_p). The size of α_p phase is approximately 39 μm. The XRD pattern exhibits strong β phase peaks, and the peaks of α phase and weak ω phase, demonstrating that $\beta+\alpha_p+\omega_{ath}$ was maintained after the solution treated at 800 °C for 2 h. This result is consistent with other β-Ti alloys [32−35].

3.2 Age hardening and precipitation sequence

The quenched Ti−6Cr−5Mo−5V−4Al alloy samples were aged at 300, 350, 400, 450, 500, 550, 580 and 600 °C. The age-hardening curves are shown in Fig. 3. From the age-hardening curve, with the increase of ageing time, the hardening hardly occurred at 300 °C. This indicates an insufficient nucleation for the precipitation of secondary phase at lower temperature. For samples aged at higher temperatures (350 and 450 °C), and a

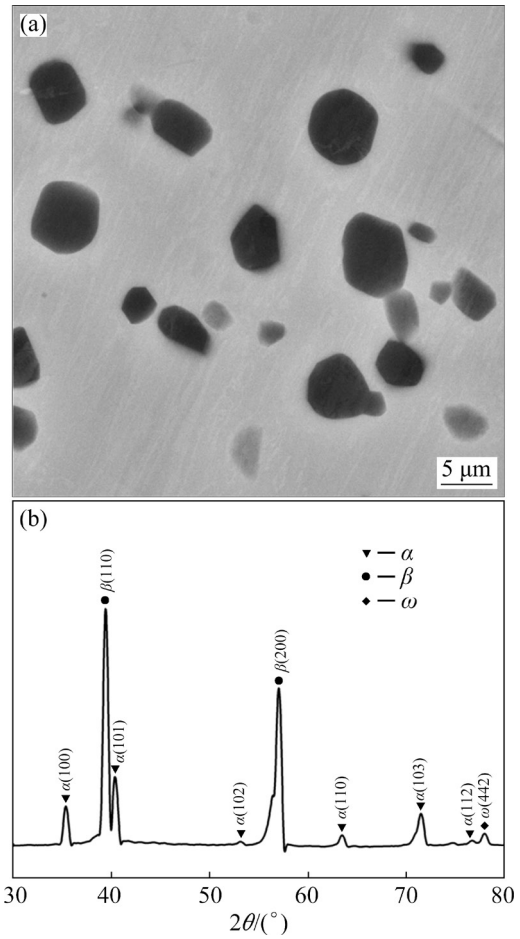

Fig. 2 SEM image (a) and XRD pattern (b) of Ti−6Cr−5Mo−5V−4Al alloy solution treated at 800 °C for 2 h

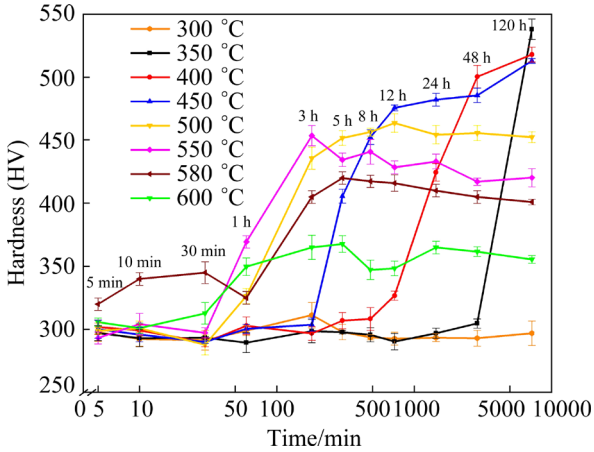

Fig. 3 Age-hardening curves of Ti−6Cr−5Mo−5V−4Al alloy solution treated at 800 °C for 2 h

prolonged ageing time of 120 h, the hardness increased to HV 538 (350 °C), HV 517 (400 °C), and HV 512 (450 °C). The alloy did not possibly reach peak ageing even after 120 h. For samples aged at 500 °C, the peak ageing occurred at 12 h with a hardness of HV 463. When the ageing

temperature reached 550 °C, the peak ageing occurred earlier at 3 h with hardness of HV 453. At higher ageing temperature, the hardness increased to peak value (HV 420 for 580 °C and HV 367 for 600 °C) at 5 h, which was lower than that at 550 °C. With increasing the ageing temperature, the peak-ageing time shortened, indicating that the driving force for secondary phase precipitation at low temperature is insufficient. When these samples were aged at low temperatures (350−450 °C), the peak value was much higher than that at higher temperatures (500−600 °C).

The evolution of phase components during ageing is revealed by XRD patterns and shown in Fig. 4. In Figs. 4(a) and (b), α, β and ω_{iso} phases were observed for samples aged at 400 and 450 °C for different ageing time. The relative intensity of β phase was lower than that in ST sample (Fig. 2(b)), and the relative intensity of the α and ω_{iso} phases increased with increasing ageing time. This infers that β phase transformed into α_s and ω_{iso} phases during ageing ($\beta + \alpha_p + \omega_{ath} \rightarrow \beta + \alpha + \omega_{iso}$), which

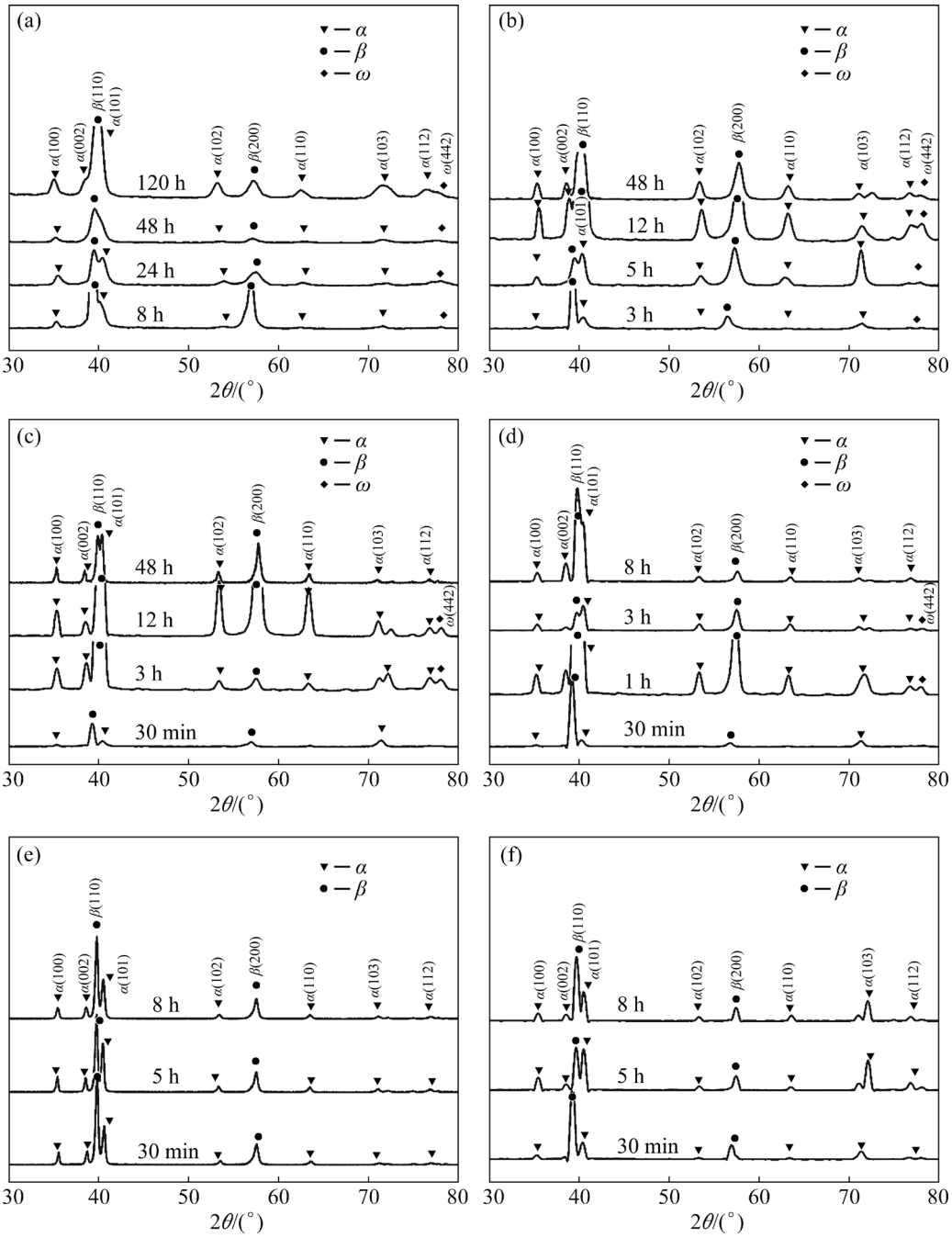

Fig. 4 XRD patterns of samples aged at different temperatures for different time: (a) 400 °C; (b) 450 °C; (c) 500 °C; (d) 550 °C; (e) 580 °C; (f) 600 °C

is consistent with the hardening curve in Fig. 3. Previous studies on Ti alloys also found the similar microstructure composed of ω_{iso} phase at relatively low ageing temperature, considering that α is difficult to precipitate directly [20,36,37]. Due to the presence of α_p phase, the precipitate of α_s phase could not be determined. As shown in Figs. 4(c, d), ω_{iso} phase gradually dissolved after 12 h at 500 °C and 3 h at 550 °C, accompanied by the precipitation of α phase. This infers a precipitation sequence, $\beta+\alpha_p+\omega_{ath}\rightarrow\beta+\alpha+\omega_{iso}\rightarrow\beta+\alpha$. The phase transformation is consistent with the hardening curve in Fig. 3. After ageing at 500 °C for 12 h and 550 °C for 3 h, the hardness curve gradually decreased because the strengthening effect of α_s phase is weaker than that of ω_{iso} phase. The ω_{iso} phase disappeared with time, and higher ageing temperature increased the disappearance rate of ω_{iso} phase. This is consistent with the hardness curve, where peak ageing at low temperature was higher than that at high temperature. When ageing at 580 and 600 °C, ω_{iso} phase does not appear, indicating that ω_{iso} phase only occurs at low temperature with the precipitation sequence, $\beta+\alpha+\omega_{ath}\rightarrow\beta+\alpha$. The precipitation sequence is summarized as

400−450 °C: $\beta+\alpha_p+\omega_{ath}\rightarrow\beta+\alpha+\omega_{iso}$

500−550 °C: $\beta+\alpha_p+\omega_{ath}\rightarrow\beta+\alpha+\omega_{iso}\rightarrow\beta+\alpha$

580−600 °C: $\beta+\alpha_p+\omega_{ath}\rightarrow\beta+\alpha$

WAN et al [19] studied the precipitation sequence of Ti−19Nb−1.5Mo−4Zr−8Sn alloy. During ageing at 400−600 °C, α'' phase precipitated rapidly within 10 min. Metastable ω formed with increasing ageing time at the low temperatures of 400−450 °C. The precipitation sequence of the alloy was determined as $\beta+\alpha'\rightarrow\omega+\alpha+\alpha''+\beta\rightarrow\alpha+\alpha''+\beta\rightarrow\alpha+\beta$ at 400−450 °C, $\beta+\alpha'\rightarrow\alpha''+\alpha+\beta\rightarrow\alpha+\beta$ at 500−600 °C. YI et al [20] found that the precipitation sequences of Ti−7Nb−10Mo during isothermal ageing at different temperatures were $\beta+\omega_{ath}\rightarrow\beta+\omega_{iso}$ (144 h) at 350−400 °C, $\beta+\omega_{ath}\rightarrow\beta+\omega_{iso}+\alpha\rightarrow\beta+\alpha$ at 500 °C, and $\beta+\omega_{ath}\rightarrow\beta+\alpha$ at 600−650 °C. LIN et al [38] found that the precipitation sequence of Ti−40Ta−22Hf−11.7Zr was determined as $\beta\rightarrow\alpha''+\beta\rightarrow\alpha+\alpha''+\beta\rightarrow\alpha+\beta$ at 300 °C. The results show that α''_{iso} precipitated below the martensitic transition initiation temperature (M_s) after ageing. The increase of β-stabilizing elements would increase the stability of β phase, and inhibit the $\beta\rightarrow\alpha''$ transition. The alloy contained higher β-stabilizing elements would lead to the reduction of M_s, and caused the formation of ω phase directly.

3.3 Precipitation of α_s phase

The SEM results in Figs. 5−7 show the microstructures of samples aged at 400−580 °C. Microstructural analysis results of the size and volume fraction of α phase are listed in Table 1. When the ageing temperature was 400 °C, the time of three samples was selected as 12 (without hardening), 48 and 120 h (with evident hardening), as shown in Figs. 5(a−c). There is no difference between the morphology of the samples aged at 400 °C and those of solution state, as shown in Figs. 5(a) and (b). After ageing at 400 °C for 120 h, only a few needle-like α_s phase appeared, as shown in Fig. 5(c). The volume fraction (VF) of α_s phase was only 6.9%, the length and width of α_s phase were about 1.27 and 0.02 μm, respectively (Table 1). The results in Figs. 3 and 5 illustrate that the hardness of the alloy aged at 400 °C for 48 and 120 h increased significantly because of the precipitation of ω_{iso} phase at low temperature.

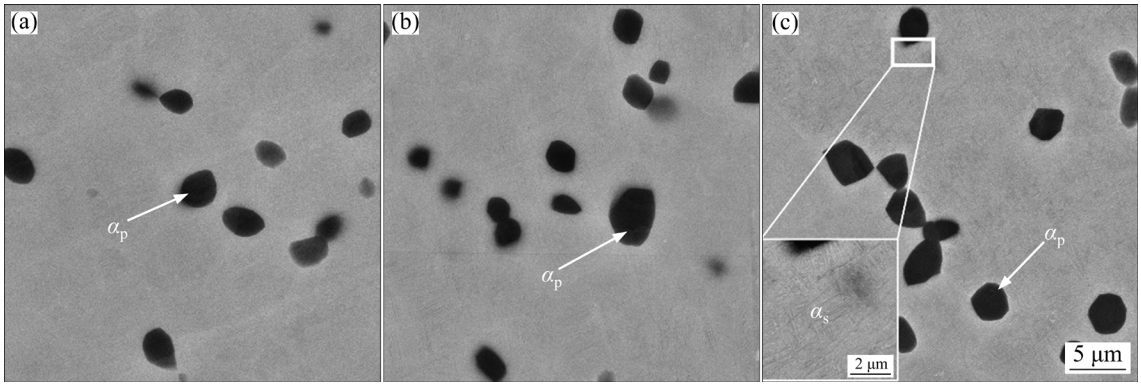

Fig. 5 Microstructures of alloy aged at 400 °C for 12 h (a), 48 h (b), and 120 h (c)

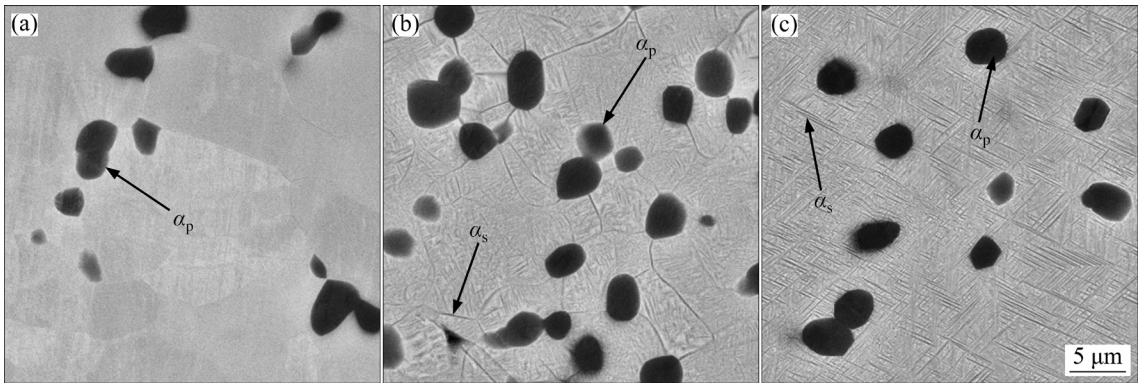

Fig. 6 Microstructures of alloy after ageing at 500 °C for 1 h (a), 12 h (b), and 48 h (c)

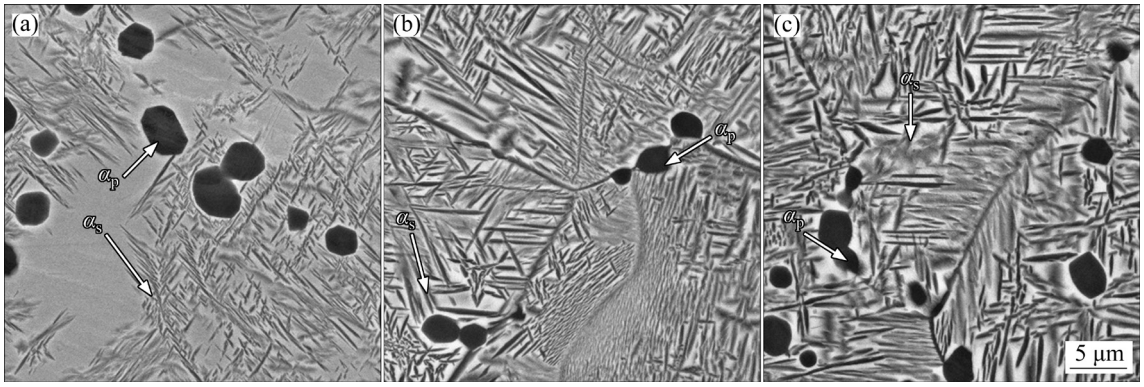

Fig. 7 Microstructures of alloy after ageing at 580 °C for 1 h (a), 5 h (b), and 24 h (c)

Table 1 Volume fraction and size of α phase after ageing

Temperature/°C	Time/h	Volume fraction of α/%		Size of α/μm		
		Primary α	Secondary α	Primary α	Secondary α	
				Width	Length	Width
400	12	9.59	–	1.67	–	–
	48	12.41	–	1.64	–	–
	120	15.13	6.9	1.76	1.27	0.02
500	1	10.22	–	1.60	–	–
	12	18.96	30.36	1.56	1.47	0.02
	48	18.13	77.06	1.64	1.76	0.04
580	1	9.93	25.67	1.76	1.33	0.09
	5	9.11	69.35	1.27	3.03	0.20
	24	12.89	69.72	1.19	3.01	0.34

When the ageing temperature increased to 500 °C, the ageing time has a significant influence on the microstructure (Fig. 6). Shorter ageing time (1 h) did not have obvious effect on α_s phase and hardening. When the ageing time was 12 h, needle-like α_s phase precipitated and the hardness increased to HV 464. When the ageing time increased to 48 h, α_s phase grew to larger size [39]. The volume fraction of α_s phase increased from 30.36% to 77.06%, the length and width of α_s phase increased from 1.47 and 0.02 μm to 1.76 and 0.04 μm, respectively, while the hardness decreased

to HV 456. These results indicate that the hardness could be improved by increasing the volume fraction and size of α_s phase at the early stage of ageing, but the hardness decreased with the coarsening of α_s phase. The peak hardness of the alloy aged at 400 °C was higher than that at 500 °C, indicating that α_s phase affects the hardness of the alloy less than ω_{iso} phase. Therefore, controlling the volume fraction and size of α_s phase is a strategy for achieving the desired properties of the alloy.

As shown in Fig. 7, the ageing temperature significantly affects the phase morphology when ageing temperature increases to 580 °C. When aged at 500 °C for 1 h, α_s phase only precipitated locally, and the volume fraction was only 25.67%. When the ageing time was extended to 5 h, α_p phase distributed uniformly. In addition, when the ageing time increased to 24 h, the volume fraction of α_s phase increased to 69.72%, and the length and width increased to 3.01 and 0.34 μm, respectively. Compared with ageing at 400 and 500 °C, α_s phase precipitated at shorter ageing time and coarsened at 580 °C. This infers that higher ageing temperature increased the driving force for α_s precipitation and accelerated its precipitation [8,40]. As shown in Figs. 5−7 and Table 1, the volume fraction, size, and morphology of α_p phase did not change significantly, which indicates that ageing temperature and time did not affect α_p.

3.4 Precipitation of ω phase

TEM results of the samples aged at 450 °C for 12 h and the corresponding bright-field micrographs are shown in Fig. 8. The acicular phases are observed in Fig. 8(a). The selected-area electron diffraction results are shown in Fig. 8(b), which confirmed the presence of ω and α phases. The reciprocal lattice of ω phase appears at the 1/3 and 2/3$[1\,\bar{1}\,0]\beta$ positions, and ω phase is observed in the corresponding dark-field phase in Fig. 8(c). The reciprocal lattice of α phase appears at the 1/2$[1\,\bar{1}\,0]\beta$ position, and the needle-like α_s phase is observed in the corresponding dark-field phase in Fig. 8(d), which is consistent with the XRD results. The orientation relationship among ω phase, α phase, and β matrix can be inferred from the speckled crystal plane index of demarcated phase (Fig. 8(e)): $(0001)\omega//(11\bar{2}0)\alpha//(11\bar{1})\beta$, $(0\bar{1}10)\omega//(1\bar{1}00)\alpha//(112)\beta$, and $[11\bar{2}0]\omega//[0001]\alpha//[1\bar{1}0]\beta$ [41].

Figure 9 shows TEM microstructure of the alloy aged at 580 °C for 12 h and the second phase is more densely distributed. The corresponding SAD pattern obtained along the $[1\,\bar{1}\,1]$ axis only appears near the 1/2$\{110\}\beta$ position, only with the reciprocal lattice point of α phase in Fig. 9(b). This indicates that during high-temperature ageing only α phase precipitated. Due to the symmetry between hexagonal close-packed (hcp) α_s phase and body-centered cubic β, there are three α_s variants, with 60° to each other. This is consistent with the orientation relationship between α_s and β phases reported previously [32,33]. Dark field (DF) images of three α_s variants are shown in Figs. 9(d, e, f). The orientation relationship among ω, α and β phases can be inferred from the speckled crystal plane index of the demarcated phase in Fig. 9(e) as $(0001)\alpha//(110)\beta$, $(0\bar{1}11)\alpha//(1\,1\,0)\beta$, and $[\bar{2}110]\alpha//[1\,\bar{1}\,1]\beta$ [42,43].

3.5 Tensile properties

The tensile properties of the alloy solution treated at 800 °C for 2 h and different ageing temperatures for 12 h are given in Fig. 10 and Table 2. The ageing temperature had a significant effect on the tensile properties. With increasing ageing temperature, the ultimate tensile strength (UTS) of the alloy decreased with the increase of elongation. The alloy aged at 450 and 500 °C had high UTS of 1424 and 1368 MPa, but relatively low elongation of 5.7% and 5.5%, respectively. It has been shown that other metastable β titanium alloys produced similar brittle fracture after ageing at low temperatures [44−46]. The precipitation of ω phase during low temperature ageing led to the embrittlement of the alloy. The brittleness of ω phase prevents dislocation slip, which causes dislocation to accumulate near ω phase during deformation. When the ageing temperature increased to 550 °C, the alloy had high ductility due to the absence of ω_{iso} phase. When the ageing temperature increased to 580 and 600 °C, the yield strength decreased to 1181 and 1108 MPa, respectively, and the elongation increased to 13.2% and 15.4%, respectively. Compared to the properties of sample aged at 550 °C, the reduced yield strength and increased ductility of the alloy aged at 580 and 600 °C are attributed to the coarsening of α_s phase, which is consistent with SEM results mentioned above.

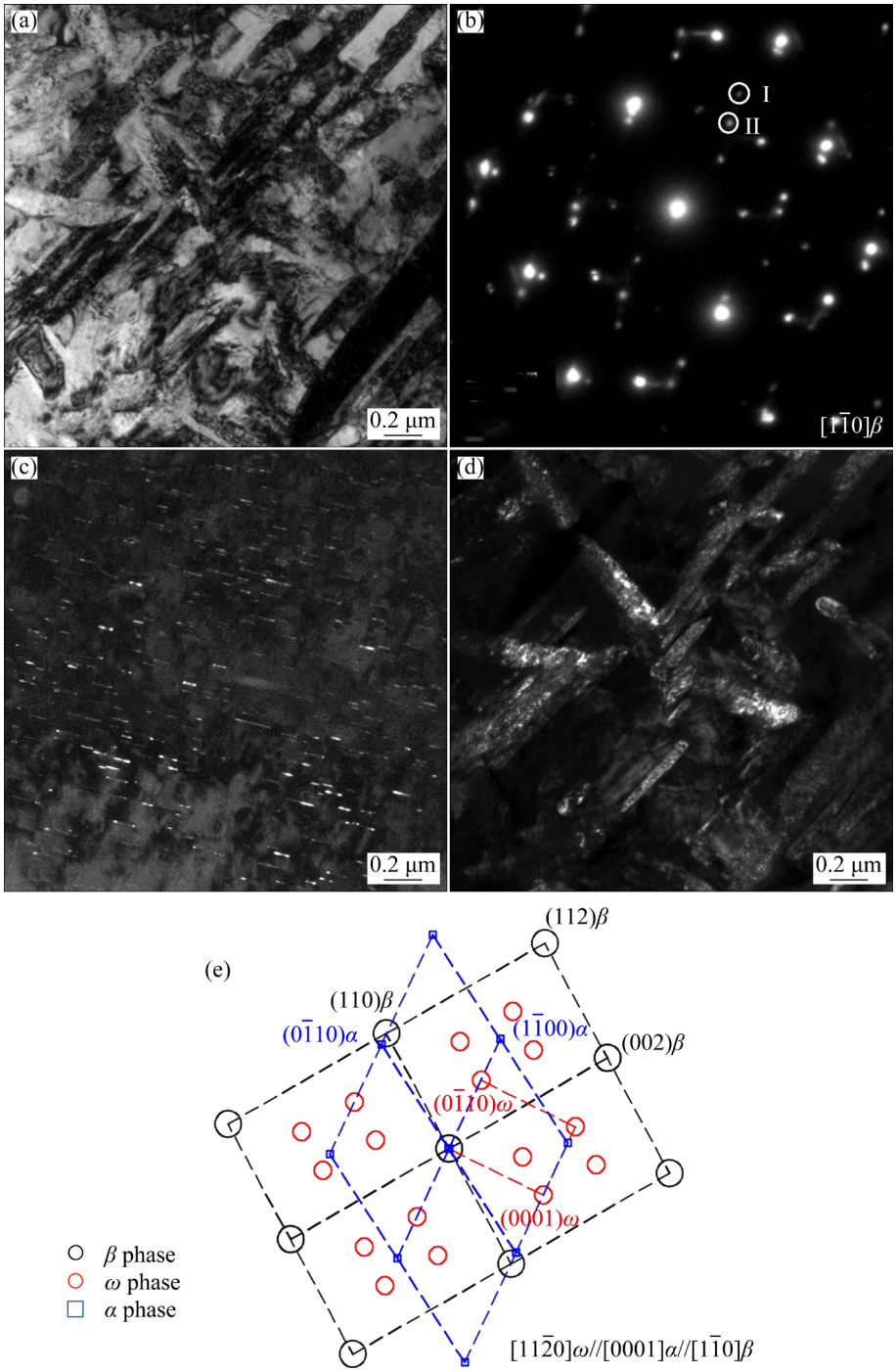

Fig. 8 TEM microstructures of alloy aged at 450 °C for 12 h: (a) Bright-field image; (b) SAD pattern along $[1\bar{1}0]\beta$ obtained from (a) (Spots I and II correspond to ω and α phases, respectively); (c) Dark-field image of Spot I in (b); (d) Dark-field image of Spot II in (b); (e) Diffraction pattern of (b)

LAI et al [44] found that after solution treatment at 900 °C, Ti−12.0Mo−0.01Fe−0.012C−0.11O alloy has excellent ductility, with an average elongation over 50% and yield strength below 526 MPa, while after ageing at 400 °C for 10 to 30 min, the yield strength increased over 900 MPa and the elongation decreased below 2% due to the precipitation of ω phase, showing the obvious embrittlement. The rejection of Mo from ω particles remarkably increases the shear modulus of the ω particles, promotes intense plastic flow localization, and facilitates crack nucleation prior to macroscopic yielding. CHEN et al [18] found that the yield strengths of Ti−19Nb−1.5Mo−4Zr−8Sn alloy after

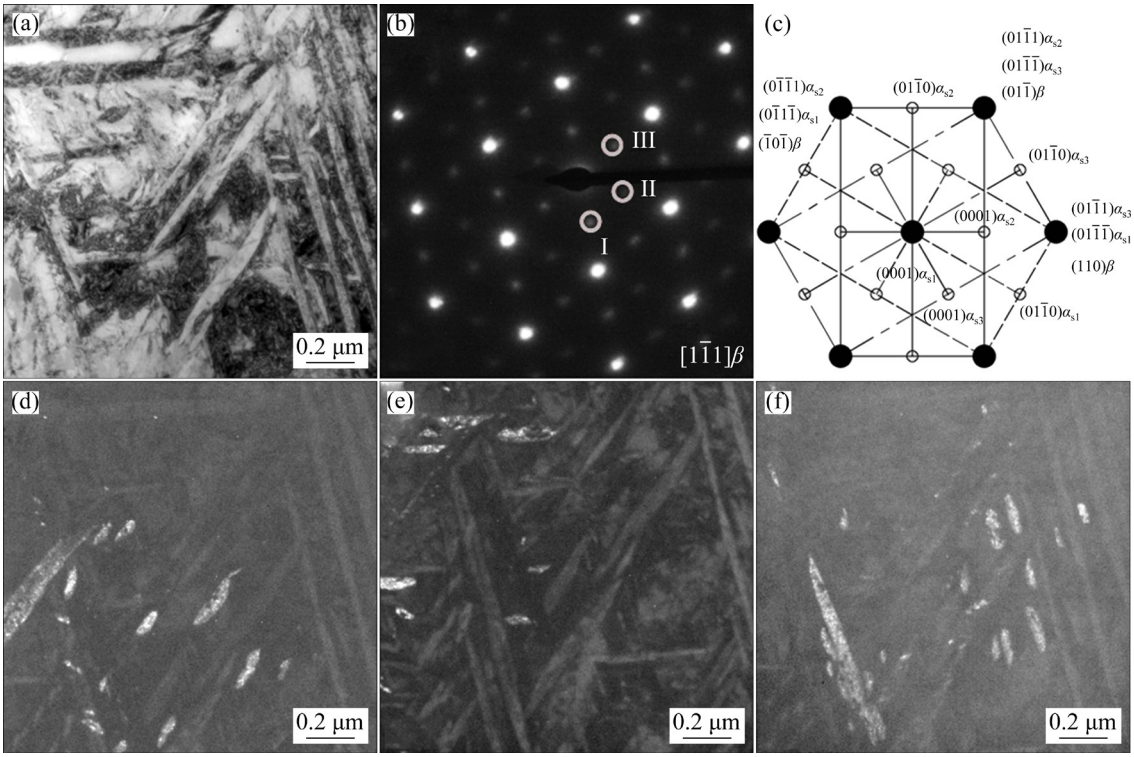

Fig. 9 TEM microstructures of sample aged at 580 °C for 12 h: (a) Bright-field image of α_s phase; (b) Corresponding SAD pattern with electron beam parallel to $[\bar{1}11]\beta$; (c) Diffraction pattern calibration of (b); (d) DF image from Spot I in (b); (e) DF image from Spot II in (b); (f) DF image from Spot III in (b)

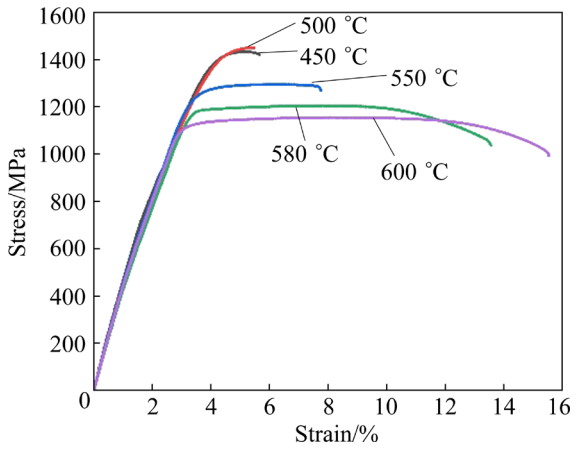

Fig. 10 Tensile stress−strain curves of samples solution treated at 800 °C followed by ageing at different temperatures for 12 h

ageing at 400 °C for 1, 10, and 30 min are 607, 725, and 786 MPa, respectively, and the corresponding elongations are 7.9%, 6.9%, and 3.9%. This was proven to be a large amount of ω phase precipitation which induced the sharp decrease of elongation lower than 4%. DONG et al [47] found that the yield strength of Ti−7Mo−3Nb−3Cr−3Al alloy aged at 600 °C was 900 MPa and the elongation was 13%. The yield strength of the alloy continuously

Table 2 Tensile properties of samples solution treated at 800 °C followed by ageing for 12 h at different temperatures

Temperature/°C	YS/MPa	TS/MPa	EL/%
450	1424	1451	5.7
500	1368	1433	5.5
550	1241	1288	7.6
580	1181	1205	13.2
600	1108	1155	15.4

heated to 600 °C was more than 1200 MPa and the elongation was below 5% due to ω precipitation. MELLO et al [48] found that when Ti−13Mo−6Sn alloy was heated slowly to the ageing temperature, the yield strength increased from 741 to 995 MPa and elongation decreased from 12% to 2.2%. This behavior was attributed to the presence of isothermal ω in the microstructure. In metastable β titanium alloys, the β phase with body-centered cubic structure contributes to the ductility of the alloy. This is due to the difficulty in activating the stress-induced martensitic phase in the α phases. The more deformation modes, the better the ductility. When α_s phase precipitates in β matrix

under ageing condition, β phase hardly undergos stress-induced martensite transformation except dislocation slip. This results in a significant increase in strength and a significant decrease in ductility due to the dispersion strengthening of the α precipitates.

Figure 11 shows the fracture morphology of tensile sample solution treated at 800 °C for 2 h followed by ageing. In Fig. 11(a), the typical mixed failure mode is shown, but the brittle failure mode was dominant, which is consistent with the higher brittleness and lower ductility compared to other samples. After low temperature ageing (450 °C), there is a large number of smooth cleavage surface, and a small number of dimples and cracks can be found. The cleavage facets and the corresponding expanded image are shown in Fig. 11(a_1). The micro-crack and dimples, and the corresponding high magnification image are shown in Fig. 11(a_2). The area fraction of the planar regions was estimated to be above 60%, and the dimples are shallow with variable size. In Fig. 11(b), when ageing at 550 °C,

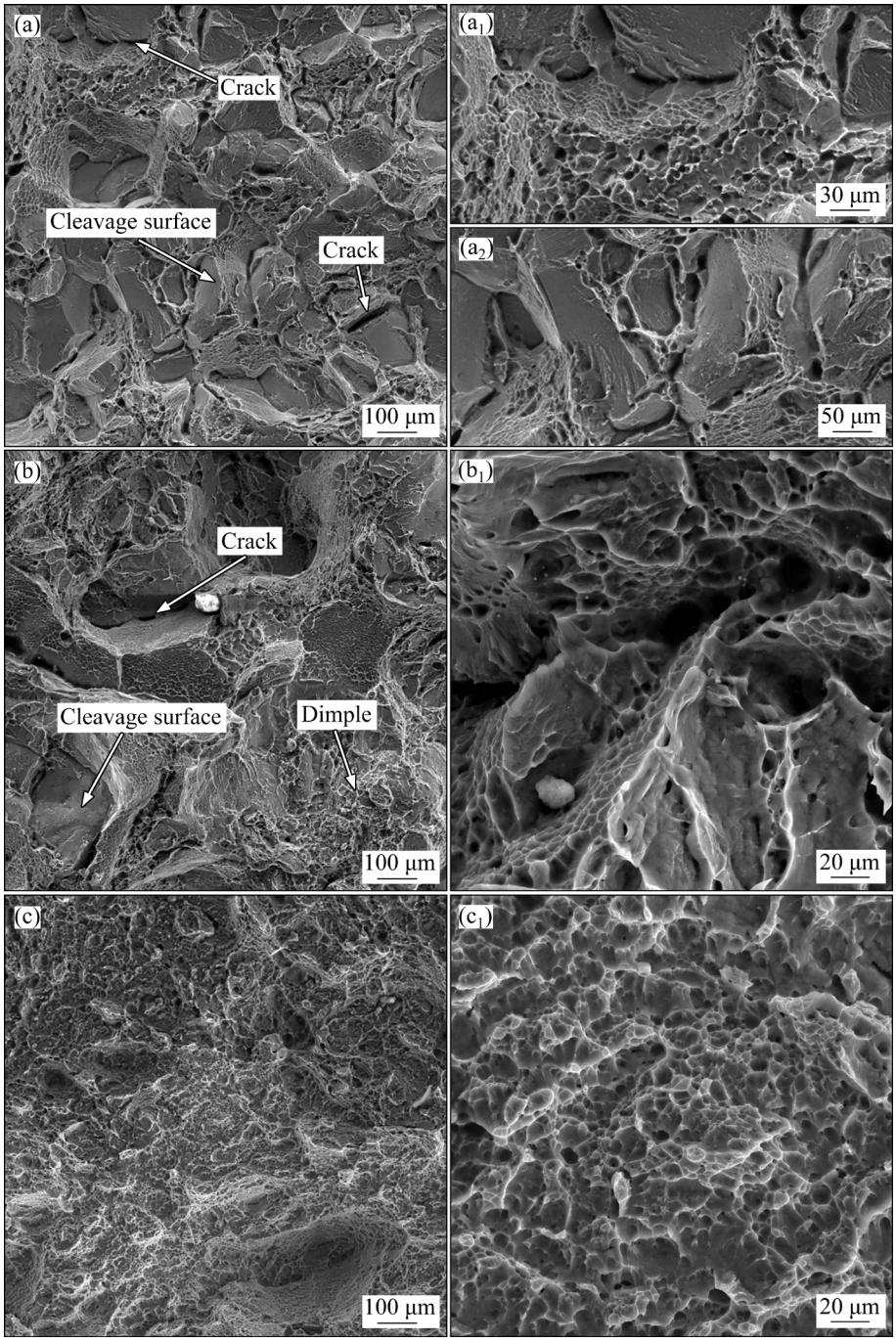

Fig. 11 Fracture surface morphologies of samples solution treated at 800 °C for 2 h, followed by ageing at different temperature for 12 h: (a) 450 °C; (b) 550 °C; (c) 580 °C; (a_1, a_2, b_1, c_1) Enlarged views of (a, b, c), respectively

the cleavage surface decreased and dimples increased. In Fig. 11(c), when ageing at 580 °C, both of plastic and brittle fractures were still observed, although the cleavage surface and microcrack were barely visible. When the number of dimple regions increased, the dimples were shallow with variable size shown in Fig. 11(c_1). As known from Fig. 8, ductility increased with increasing ageing temperature, although the strength decreased, which was related to the thickness of α_s. With the increase of α_s, the difficulty of crack propagation along the path increased. As a result, the propagation path became more tortuous as zigzag pattern, thus, the crack required more energy to bypass the α_s phase. This improves crack propagation resistance and ductility.

4 Conclusions

(1) The solution-treated alloy exhibits a circular α phase and a small amount of ω_{ath} phase in the β matrix. After ageing at 400−450 °C, ω_{iso} phase precipitates in matrix. With the increase of ageing temperature, ω_{iso} phase gradually transformed to α_s phase. At higher ageing temperature (580−600 °C), ω_{iso} precipitation is suppressed, and α_s phase precipitated directly from β phase. At 400 °C, α_s precipitated after ageing for 120 h, while at higher ageing temperature α_s precipitated during the early ageing stage.

(2) The increase of ageing time accelerates the precipitation and coarsening of α_s phase. Ageing at low temperature should be avoided in order to mitigate brittleness by the precipitation of a large amount of ω phase, although very high strength could be achieved.

(3) The orientation relation among ω, α, and β phases could be inferred as $(0001)\omega//(11\bar{2}0)\alpha//(11\bar{1})\beta$, $(0\bar{1}10)\omega//(1\bar{1}00)\alpha//(112)\beta$, and $[11\bar{2}0]\omega//[0001]\alpha//[1\bar{1}0]\beta$. The precipitation sequences during ageing are as: (400−450 °C) $\beta+\alpha_p+\omega_{ath}\rightarrow\beta+\alpha_p+\alpha_s+\omega_{iso}$; (500−550 °C) $\beta+\alpha_p+\omega_{ath}\rightarrow\beta+\alpha_p+\alpha_s+\omega_{iso}\rightarrow\beta+\alpha_p+\alpha_s$; (580−600 °C) $\beta+\alpha_p+\omega_{ath}\rightarrow\beta+\alpha_p+\alpha_s$.

Acknowledgments

This research was funded by the National Key Research and Development Program of China (No. 2021YFB3700801), and by the State Key Laboratory of Powder Metallurgy, Central South University, Changsha, China.

References

[1] XU Jian-wei, ZENG Wei-dong, ZHOU Da-di, HE Sheng-tong, JIA Run-chen. Evolution of coordination between α and β phases for two-phase titanium alloy during hot working [J]. Transactions of Nonferrous Metals Society of China, 2021, 31: 3428−3438.

[2] WANG Ke, WU Ming-yu, REN Zhao, ZHANG Yu, XIN Ren-long, LIU Qing. Static globularization and grain morphology evolution of α and β phases during annealing of hot-rolled TC21 titanium alloy [J]. Transactions of Nonferrous Metals Society of China, 2021, 31: 2664−2676.

[3] YUMAK N, ASLANTAŞ K. A review on heat treatment efficiency in metastable β titanium alloys: The role of treatment process and parameters [J]. Journal of Materials Research and Technology, 2020, 9: 15360−15380.

[4] ZHU Yan-yan, CHEN Bo, TANG Hai-bo, CHENG Xu, WANG Hua-ming, LI Jia. Influence of heat treatments on microstructure and mechanical properties of laser additive manufacturing Ti−5Al−2Sn−2Zr−4Mo−4Cr titanium alloy [J]. Transactions of Nonferrous Metals Society of China, 2018, 28: 36−46.

[5] ZHOU Zhong-bo, FEI Yue, LAI Min-jie, KOU Hong-chao, CHANG Hui, SHANG Guo-qiang, ZHU Zhi-shou, LI Jin-shan, ZHOU Lian. Microstructure and mechanical properties of new metastable β type titanium alloy [J]. Transactions of Nonferrous Metals Society of China, 2010, 20: 2253−2258.

[6] YOUSSEF S S, ZHENG Xiao-dong, MA Ying-jie, HUANG Sen-sen, QI Min, QIU Jian-ke, ZHANG Rui-xue, HUA Pei-tao, ZHENG Shi-jian, LEI Jia-feng, YANG Rui. Characterization of α_2 Precipitates in Ti−6Al and Ti−8Al binary alloys: A comparative investigation [J]. Acta Metallurgica Sinica (English Letters), 2021, 34: 710−718.

[7] SHI Zhi-feng, GUO Hong-zhen, ZHANG Jian-wei, YIN Jian-ning. Microstructure−fracture toughness relationships and toughening mechanism of TC21 titanium alloy with lamellar microstructure [J]. Transactions of Nonferrous Metals Society of China, 2018, 28: 2440−2448.

[8] SUN Hong, YU Li-ming, LIU Yong-chang, ZHANG Li-ye, LIU Chen-xi, LI Hui-jun, WU Jie-feng. Effect of heat treatment processing on microstructure and tensile properties of Ti−6Al−4V−10Nb alloy [J]. Transactions of Nonferrous Metals Society of China, 2019, 29: 59−66.

[9] DU Z X, GUO H, LIU J W, CHENG J, ZHAO X P, WANG X P, LIU F, CUI X M. Microstructure evolution during aging heat treatment and its effects on tensile properties and dynamic Young's modulus of a biomedical β titanium alloy [J]. Materials Science and Engineering: A, 2020, 791: 139677.

[10] ZHANG Su-jie, MIN Xiao-hua, LI Ya-da, WANG Wei-qiang, LI Ping, LI Ming-jia. Effects of deformation and phase transformation microstructures on springback behavior and biocompatibility in β-type Ti−15Mo alloy [J]. Acta Metallurgica Sinica (English Letters), 2022, 35: 621−635.

[11] WANG Zhen-yu, LIU Li-bin, WU Di, ZHANG Li-gang, WANG Wan-lin, ZHOU Ke-chao. α'' phase-assisted nucleation to obtain ultrafine α precipitates for designing high-strength near-β titanium alloys [J]. Transactions of Nonferrous Metals Society of China, 2020, 30: 2681−2696.

[12] ZHOU L B, SUN J S, ZHANG R Z, CHEN J, HE J J, YUAN T C. A new insight into the α phase precipitation in β titanium alloy [J]. Vacuum, 2021, 189: 110272.

[13] ZHU Wen-guang, LEI Jia, TAN Chang-sheng, SUN Qiao-yan, CHEN Wei, XIAO Lin, SUN Jun. A novel high-strength β-Ti alloy with hierarchical distribution of α-phase: The superior combination of strength and ductility [J]. Materials & Design, 2019, 168: 107640.

[14] YI Hui-Jun, LEE Yong-Jun, LEE Kwang-O. Influences of the welding heat input and the repeated repair welding on Ti−3Al−2.5V titanium alloy [J]. Acta Metallurgica Sinica (English Letters), 2015, 28: 684−691.

[15] XIANG Li, MIN Xiao-hua, JI Xin, EMURA S, CHENG Cong-qian, TSUCHIYA K. Effect of pre-cold rolling-induced twins and subsequent precipitated ω-phase on mechanical properties in a β-type Ti−Mo alloy [J]. Acta Metallurgica Sinica (English Letters), 2018, 31: 604−614.

[16] CHEN Wei, CAO Shuo, ZHANG Jin-yu, ZHA You, HU Qing-miao, SUN Jun. New insights into ω-embrittlement in high misfit metastable β-titanium alloys: Mechanically-driven ω-mediated amorphization [J]. Materials & Design, 2021, 205: 109724.

[17] WANG Kai-ge, WU Di, WANG Dong, DENG Zi-xuan, TIAN Yue-yan, ZHANG Li-gang, LIU Li-bin. Influence of cooling rate on ω phase precipitation and deformation mechanism of a novel metastable β titanium alloy [J]. Materials Science and Engineering A, 2022, 829: 142151.

[18] CHEN Wei, CAO Shuo, KOU Wen-juan, ZHANG Jin-yu, WANG Yue, ZHA You, PAN Yan, HU Qing-miao, SUN Qiao-yan, SUN Jun. Origin of the ductile-to-brittle transition of metastable β-titanium alloys: Self-hardening of ω-precipitates [J]. Acta Materialia, 2019, 170: 187−204.

[19] WAN Wei-feng, LIU Hui-qun, JIANG Yong, YI Dan-qing, YI Ruo-wei, GAO Qi, WANG Ding-chun, YANG Qi. Microstructure characterization and property tailoring of a biomedical Ti−19Nb−1.5Mo−4Zr−8Sn alloy [J]. Materials Science and Engineering: A, 2015, 637: 130−138.

[20] YI R W, LIU H Q, YI D Q, WAN W E, WANG B, JIANG Y, WANG Q, QI Y, WANG D C, GAO Q, XU Y F, TANG Q. Precipitation hardening and microstructure evolution of the Ti−7Nb−10Mo alloy during aging [J]. Materials Science and Engineering: C, 2016, 63: 577−586.

[21] KOU Hong-chao, ZHANG Han-lei, CHU Yu-dong, HUANG Dong, NAN Hai, LI Jin-shan. Microstructure evolution and phase transformation of Ti−6.5Al−2Zr−Mo−V alloy during thermohydrogen treatment [J]. Acta Metallurgica Sinica (English Letters), 2015, 28: 505−513.

[22] ZHANG Zhi-qing, XU Huan-huan, WU Sai-nan, LIU Yin. Effects of combined pre-straining and pre-aging on natural aging and bakehardening response of an Al−Mg−Si alloy [J]. Acta Metallurgica Sinica (English Letters), 2013, 26: 340−344.

[23] WU Chuan, ZHAN Mei. Microstructural evolution, mechanical properties and fracture toughness of near β titanium alloy during different solution plus aging heat treatments [J]. Journal of Alloys and Compounds, 2019, 805: 1144−1160.

[24] WU Chuan, ZHAN Mei. Effect of solution plus aging heat treatment on microstructural evolution and mechanical properties of near-β titanium alloy [J]. Transactions of Nonferrous Metals Society of China, 2019, 29: 997−1006.

[25] ZHU Wen-guang, LI Pei, SUN Xun, CHEN Wei, ZHANG Hua-lei, SUN Qiao-yan, LIU Bin, XIAO Lin, SUN Jun. Precipitation response and hardening behaviors of Fe-modified Ti5553 alloy [J]. Transactions of Nonferrous Metals Society of China, 2019, 29: 1242−1251.

[26] ZHU Wen-guang, LEI Jia, SU Bin, SUN Qiao-yan. The interdependence of microstructure, strength and fracture toughness in a novel β titanium alloy Ti−5Al−4Zr−8Mo−7V [J]. Materials Science and Engineering: A, 2020, 782: 139248.

[27] KENT D, WANG G, WANG W, DARGUSCH M S. Influence of ageing temperature and heating rate on the properties and microstructure of β Ti alloy, Ti−6Cr−5Mo−5V−4Al [J]. Materials Science and Engineering: A, 2012, 531: 98−106.

[28] GU Kan, ZENG Xiao-qin, CHEN Bin, WANG Ying-xin. Effect of double aging on mechanical properties and microstructure of EV31A alloy [J]. Transactions of Nonferrous Metals Society of China, 2021, 31: 2606−2614.

[29] LI Chang, XIONG Han-qing, BHATTA L, WANG Lin, ZHANG Zhao-yang, WANG Hui, KONG C, YU Hai-liang. Microstructure evolution and mechanical properties of Al−3.6Cu−1Li alloy via cryorolling and aging [J]. Transactions of Nonferrous Metals Society of China, 2020, 30: 2904−2914.

[30] ZHAN Hong-yi, KENT D, WANG Gui, DARGUSCH M S. The dynamic response of a β titanium alloy to high strain rates and elevated temperatures [J]. Materials Science and Engineering: A, 2014, 607: 417−426.

[31] LIU Tian-wen, WANG Qu-dong, TANG Hua-ping, LI Zhong-yang, LEI Chuan, EBRAHIMI M, JIANG Hai-yan, DING Wen-Jiang. Microstructure and mechanical properties of squeeze-cast Al−5.0Mg−3.0Zn−1.0Cu alloys in solution-treated and aged conditions [J]. Transactions of Nonferrous Metals Society of China, 2020, 30: 2326−2338.

[32] XIAO J F, NIE Z H, TAN C W, ZHOU G, CHEN R, LI M R, YU X D, ZHAO X C, HUI S X, YE W J, LEE Y T. Effect of reverse β-to-ω transformation on twinning and martensitic transformation in a metastable β titanium alloy [J]. Materials Science and Engineering: A, 2019, 759: 680−687.

[33] LIN Cheng, YIN Gui-li, ZHANG Ai-min, ZHAO Yong-qing, LI Qing-chun. Simple models to account for the formation and decomposition of athermal ω phase in titanium alloys [J]. Scripta Materialia, 2016, 117: 28−31.

[34] LIU Hui-hong, NIINOMI M, NAKAI M, CHO K. Athermal and deformation-induced ω-phase transformations in biomedical beta-type alloy Ti−9Cr−0.2O [J]. Acta Materialia, 2016, 106: 162−170.

[35] HASHMI M L, WADOOD A. Microstructural, mechanical and shape memory characterizations of Ti–Mo–Sn alloys [J]. Transactions of Nonferrous Metals Society of China, 2020, 30: 688−700.

[36] VISHNU J, SANKAR M, RACK H J, RAO N, SINGH A K, MANIVASAGAM G. Effect of phase transformations during aging on tensile strength and ductility of metastable beta titanium alloy Ti−35Nb−7Zr−5Ta−0.35O for orthopedic applications [J]. Materials Science and Engineering: A, 2020, 779: 139127.
[37] DU Zhao-xin, MA Yan, LIU Fei, ZHAO Xue-ping, CHEN Yan-fei, LI Guo-wei, LIU Guo-long, CHEN Yu-yong. Improving mechanical properties of near beta titanium alloy by high-low duplex aging [J]. Materials Science and Engineering: A, 2019, 754: 702−707.
[38] LIN J X, OZAN S, MUNIR K, WANG K, TONG X, LI Y C, LI G Y, WEN C E. Effects of solution treatment and aging on the microstructure, mechanical properties, and corrosion resistance of a β type Ti−Ta−Hf−Zr alloy [J]. RSC Advances, 2017, 7: 12309−12317.
[39] HUSSEIN M, ADESINA A Y, KUMAR M, AZEEM M, SOROUR A, AL-AQEELI N. Improvement of in vitro corrosion, wear, and mechanical properties of newly developed Ti alloy by thermal treatment for dental applications [J]. Transactions of Nonferrous Metals Society of China, 2021, 31: 952−966.
[40] CHEN Kui-wai, PAN Su-ping, LIU Hui-qun, JIANG Yong. Effect of α phase morphology on fatigue crack growth behavior of Ti−5Al−5Mo−5V−1Cr−1Fe alloy [J]. Transactions of Nonferrous Metals Society of China, 2020, 30: 2459−2471.
[41] PRIMA F, VERMAUT P, TEXIER G, ANSEL D, GLORIANT T. Evidence of α-nanophase heterogeneous nucleation from ω particles in a β-metastable Ti-based alloy by high-resolution electron microscopy [J]. Scripta Materialia, 2006, 54: 645−648.
[42] NAG S, BANERJEE R, SRINIVASAN R, HWANG J Y, HARPER M, FRASER H L. ω-Assisted nucleation and growth of α precipitates in the Ti–5Al–5Mo–5V–3Cr–0.5Fe β titanium alloy [J]. Acta Materialia, 2009, 57: 2136−2147.
[43] WU Zhi-hong, KOU Hong-chao, CHEN Na-na, HUA Ke, ZHANG Meng-qi, FAN Jiang-kun, TANG Bin, LI Jin-shan. The effects of grain morphology and crystallographic orientation on fatigue crack initiation in a metastable β titanium alloy Ti-7333 [J]. Materials Science and Engineering: A, 2020, 798: 140222.
[44] LAI M J, LI T, YAN F K, LI J S, RAABE D. Revisiting ω phase embrittlement in metastable β titanium alloys: Role of elemental partitioning [J]. Scripta Materialia, 2021, 193: 38−42.
[45] CHOU K, LI Nan, MARQUIS E A. Enhanced work hardening from oxygen-stabilized ω precipitates in an aged metastable β Ti−Nb alloy [J]. Acta Materialia, 2021, 220: 117302.
[46] ZHANG Rui-xue, MA Ying-jie, QI Min, HUANG Sen-sen, YOUSSEF S S, XI Guo-qiang, QIU Jian-ke, LEI Jia-feng, YANG Rui, WANG Ping. The effect of precursory α and ω phase on microstructure evolution and tensile properties of metastable β titanium alloy [J]. Journal of Materials Research and Technology, 2022, 16: 912−921.
[47] DONG Rui-feng, LI Jin-shan, KOU Hong-chao, FAN Jiang-kun, ZHAO Yu-hong, HOU Hua, WU Li. ω-Assisted refinement of α phase and its effect on the tensile properties of a near β titanium alloy [J]. Journal of Materials Science & Technology, 2020, 44: 24−30.
[48] de MELLO M G, SALVADOR C A F, FANTON L, CARAM R. High strength biomedical Ti−13Mo−6Sn alloy: Processing routes, microstructural evolution and mechanical behavior [J]. Materials Science and Engineering: A, 2019, 764: 138190.

亚稳 β 型 Ti−6Cr−5Mo−5V−4Al 合金的时效析出序列及 ω 和次生 α 相对拉伸性能的影响

周 薇[1]，汪 畅[1]，刘继雄[2]，李斯韫[3]，刘会群[1,3]

1. 中南大学 材料科学与工程学院，长沙 410083；
2. 宝钛集团有限公司，宝鸡 721014；
3. 中南大学 粉末冶金国家重点实验室，长沙 410083

摘 要：研究亚稳 β 型钛合金 Ti−6Cr−5Mo−5V−4Al 固溶和时效过程中的析出序列及显微组织和拉伸性能之间的关系。在 400~450 ℃时效时，合金析出等温 ω 相(ω_{iso})，引起高硬化行为和脆性断裂。在 450~500 ℃时效时，随时效时间增加，ω_{iso} 相逐渐演化为次生 α 相(α_s)。在更高温度(580~600 ℃)时效时，ω_{iso} 相析出受到抑制，α_s 相直接从 β 相析出。由于 ω_{iso} 相析出，合金在 450 ℃时效 12 h 时的屈服强度为 1368 MPa，伸长率为 5.5%。随 α_s 相析出和粗化，合金在 600 ℃时效 12 h 时的屈服强度为 1108 MPa，伸长率提高到 15.4%。

关键词：亚稳态 β-Ti 合金；时效序列；ω 相；α_s 相；强度；塑性

(Edited by Xiang-qun LI)